Colloid and Interface Science Communications 72 (2026) 100885

Contents lists available at ScienceDirect

Colloid and Interface Science Communications

journal homepage: www.elsevier.com/locate/colcom

Interfacial plasmon engineering in bamboo/PVA/chitosan nanofibers: Laser-ablated Au nanoparticles for visible-light photocatalytic water treatment☆

Yasemin Gündoğdu Kabakci [a,b,c], Nezihe Mehtap [a], M.A.Basyooni-M. Kabatas [d,e,f,*], Hamdi Şükür Kiliç [g]

[a] Department of Physics, Faculty of Science, Selçuk University, Konya 42075, Turkey
[b] Laser Induced Proton Therapy Application and Research Center, Selçuk University, Konya 42075, Turkey
[c] High Technology Research and Application Center, Selçuk University, Konya 42075, Turkey
[d] Department of Precision and Microsystems Engineering, Delft University of Technology, Mekelweg 2, 2628 CD Delft, the Netherlands
[e] Institute of Nanotechnology, Karlsruhe Institute of Technology, Kaiserstraße 12, 76131 Karlsruhe, Germany
[f] Department of Nanotechnology and Advanced Materials, Graduate School of Applied and Natural Sciences, Selçuk University, Konya 42030, Turkey
[g] Department of Metallurgical and Materials Engineering, Faculty of Engineering, Dokuz Eylül University, Buca, 35160 İzmir, Turkey

ARTICLE INFO

Keywords:
Gold nanoparticles
Bamboo/PVA/chitosan nanofibers
Visible-light photocatalysis
Interfacial plasmonic engineering
Methylene blue degradation
Colloid-nanofiber interface
Sustainable water treatment

ABSTRACT

Gold nanoparticles were synthesized via surfactant-free laser ablation and incorporated into electrospun bamboo/poly(vinyl alcohol)/chitosan nanofibers for plasmonic photocatalysis. Comprehensive characterization via FE-SEM, FTIR, Raman, TGA, and UV–Vis spectroscopy revealed the synergistic integration of renewable bamboo biocomponents with laser-ablated Au nanoparticles. At pH 10, Bamboo/Au/PVA/CS-2 nanofibers achieved 70.55% methylene blue degradation in 240 min, a 1.8-fold improvement over the PVA/CS baseline (50.27%), with a pseudo-first-order rate constant of 0.0038 min^{-1}. Radical scavenger experiments confirmed that superoxide radicals ($\bullet O_2^-$) and photogenerated holes (h^+) are the dominant reactive species, thereby elucidating the SPR-assisted charge-transfer mechanism. These results demonstrate that bamboo-derived, Au-modified PVA/CS nanofibers represent a promising class of eco-friendly, plasmon-enhanced photocatalysts for sustainable water treatment, establishing an innovative platform for colloid-interface engineering in environmental remediation.

1. Introduction

Composite materials designed for photocatalytic applications have attracted increasing attention in recent years owing to their potential for environmental remediation. Among these systems, carbon-based composites are particularly appealing due to their structural stability, high electrical conductivity, and ease of functionalization. Numerous contaminants, including pesticides, organic dyes, heavy metals, microbes (bacteria, viruses, and fungi), food additives, personal care products, prescription antibiotics, and other waterborne pollutants, pose serious risks to human health [1,2]. The growing global population, together with the progressive depletion of freshwater resources, has created an urgent need for the sustainable reuse of water. Effective water reuse requires not only the efficient removal of diverse contaminants but also the development of filtration systems that are environmentally benign and based on naturally biodegradable materials. Such materials are especially important in water treatment, where minimizing ecological impact is a key priority. However, despite increasing demand, opportunities to produce cost-effective, eco-friendly composite materials remain limited.

Natural fiber-based composites have attracted significant interest in engineering applications due to their rigidity, durability, and versatility, as highlighted by Lau et al. [3]. Incorporating biodegradable fibers into polymer-reinforced composites presents a promising alternative to synthetic fibers, offering both economic and environmental benefits. Moreover, combining natural fibers with advances in nanotechnology

☆ This article is part of a Special issue entitled: 'From Colloids to Clean Energy' published in Colloid and Interface Science Communications.

* Corresponding author at: Department of Precision and Microsystems Engineering, Delft University of Technology, Mekelweg 2, 2628 CD Delft, the Netherlands.
E-mail addresses: m.kabatas@tudelft.nl, m.kabatas@kit.edu (M.A.Basyooni-M. Kabatas).

https://doi.org/10.1016/j.colcom.2026.100885
Received 13 December 2025; Received in revised form 16 February 2026; Accepted 6 March 2026
Available online 10 March 2026

opens a novel research avenue for enhancing the structural and functional properties of polymer matrices. This strategy not only addresses sustainability challenges but also supports the development of high-performance, eco-friendly engineering materials for water treatment and related applications [4,5]. Bamboo, a natural material well recognized for its intrinsic water-purification capabilities, enhances catalytic activity. It is a typical biomass resource that can be utilized as a carbon precursor. Bamboo-based carbon materials offer broad application potential owing to their high adsorption capacities for organic pollutants and metal ions [6]. Compared with other carbon precursors, such as graphene, carbon nanotubes, and fullerenes, bamboo charcoal is a cost-effective carbon source for the preparation process [7]. For example, Chou et al. fabricated bamboo charcoal/TiO_2 composites that exhibited high efficiency when applied in dye-sensitized solar cells [8]. Bamboo fibers are widely used in the textile industry for the manufacture of apparel, towels, and bathrobes due to their multifunctional properties. Due to their inherent antimicrobial properties, these materials are used in a range of medical and hygienic products, including bandages, masks, surgical gowns, and sanitary pads. Furthermore, bamboo fibers are incorporated into UV-resistant, antibacterial, and bacteriostatic textiles, including curtains, wall coverings, and various other products, to mitigate bacterial proliferation and reduce the detrimental effects of ultraviolet radiation. Chitosan (CS) has recently attracted significant attention due to its non-toxic nature, biocompatibility, and biodegradability, making it suitable for a wide range of applications. Chitosan is a polysaccharide consisting of a repeating glucosidic backbone with one amino group and two hydroxyl groups. It can be obtained by thermochemical deacetylation of chitin in an alkaline medium, as well as naturally from fungi [9]. Although it is typically produced via alkaline processes, such as hydrolysis of acetylated positions with NaOH solutions, which leads to *N*-deacetylation of chitin, additional methods, including the use of hydrazine sulfate and anhydrous hydrazine, are also employed for chitosan production [10]. The incorporation of side groups into the chitosan backbone enables the development of versatile materials with tailored functionalities, thereby modifying their biological and physical properties.

Photocatalysis is a widely used and efficient technique for pollutant removal at room temperature and ambient pressure, primarily because it generates reactive oxygen species (ROS) under light irradiation. In recent years, it has also emerged as a promising green antibacterial strategy. In this field, increasing attention has been directed toward the development of visible-light-active photocatalysts. Silver (Ag) is one of the most frequently studied visible-light-active photocatalysts because of its tunable plasmon resonance in the visible spectrum [11,12]. In a study on surface plasmon-induced photocatalysis using Au/TiO_2 nanoparticles, Gao et al. experimentally demonstrated that the plasmon-induced photocatalytic activity is enhanced when the polarization direction of light is perpendicular to the Au/TiO_2 interface [13]. For photocatalytic applications, tailoring materials by integrating different functional components into nanofibers produced via electrospinning can significantly improve their properties. For instance, cross-linked poly (vinyl alcohol) (PVA)/chitosan (CS) magnetic nanofiber membranes incorporating magnetic nanoparticles have shown enhanced efficiency in the removal of heavy metals [14]. In another approach, a poly(N-vinylpyrrolidone) (PVP) polymer template was modified via electrospinning and calcination to synthesize Au nanoparticles (Au NPs). It was found that the detection of Au NPs was improved due to electrostatic interactions between negatively charged Au NPs and positively charged aminosilane groups [15].

Interest in catalytic processes driven by localized surface plasmon resonance (LSPR) has expanded markedly over the past decade, following pioneering work on plasmon-based nanocatalysts in the early 2000s [16]. Tian and Tatsuma introduced the concept of employing plasmonic Au nanoparticles in TiO_2 films to achieve visible-light photocatalytic oxidation of methanol and ethanol, laying the groundwork for the design of new photocatalysts [17]. Subsequently, Awazu et al. coined the term “plasmonic photocatalysis” in their report on the photodecomposition of methylene blue using plasmonic Ag nanoparticles embedded in TiO_2 films [18]. Plasmonic photocatalysts typically consist of metal nanoparticles embedded in dielectric or semiconductor matrices, with particle sizes smaller than the wavelength of visible light. When the nanoparticle surface is illuminated, LSPR is excited, leading to an intensified local electromagnetic field and the generation of highly energetic charge carriers, often referred to as “hot” electrons and “hot” holes [19]. In the plasmon-mediated electron transfer (PMET) or LSPR sensitization mechanism, hot electrons are injected into the semiconductor's conduction band [20]. In addition to this process, hot carriers can directly oxidize or reduce interfacial chemical species via chemical interface damping (CID) [21]. Hot electrons transferred to the semiconductor conduction band can participate directly in surface reactions or migrate to defect sites, suppressing photoluminescence and delaying electron–hole recombination. When the semiconductor itself can be excited under visible light, as in the case of carbon nitride, holes in the valence band may also be transferred to the metallic nanoparticles. Plasmonic effects have been reported for metals such as Au, Ag, Pt, Rh, and Cu in various photocatalytic systems [22,23].

This strategy directly addresses the nano–environment interface by coupling plasmonic Au nanoparticles with a biodegradable bamboo/PVA/CS nanofiber support, enabling efficient visible-light-driven pollutant removal while minimizing secondary environmental impacts. By integrating surfactant-free, laser-generated Au nanoparticles into a renewable, bio-based matrix, the present work demonstrates how nanoscale design can be aligned with sustainability requirements in water treatment. In the present work, gold (Au) nanoparticles were synthesized by laser ablation and incorporated at two loading levels into a bamboo/poly(vinyl alcohol) (PVA)/chitosan (CS) composite matrix to form electrospun nanofibers. The photocatalytic performance of these nanofibers under visible light irradiation was systematically evaluated, with particular emphasis on the surface plasmon resonance (SPR) effect of the Au nanoparticles. Bamboo powder was used as a sustainable carbon source with intrinsic water-purification capabilities, while the biocompatible PVA/CS matrix provided mechanical integrity and processability. The primary objective of this study was to develop a cost-effective and eco-friendly nanofiber photocatalyst by combining bamboo-derived carbon with laser-ablated gold nanoparticles. The results showed that increasing the Au nanoparticle content led to a pronounced enhancement in the photocatalytic efficiency of the nanocomposite system.

2. Materials and characterizations

2.1. Preparation of bamboo fibers in powder form

Bamboo, a natural composite consisting of cellulose fibers embedded in a lignin matrix, was obtained from a commercial supplier [24]. In this study, the bamboo culms were cut into defined dimensions and dried under ambient conditions in a clean environment [25,26]. The dried pieces were then pulverized using a grinder and further processed by ball milling to obtain bamboo powder. The milling conditions were adjusted to achieve a particle size that allowed the powder to pass smoothly through the syringe needle of the electrospinning system.

2.2. Laser ablation gold nanoparticle production

Laser ablation (LA) is a technique based on the removal of material from a solid surface through laser–material interactions and has been widely employed for nanoparticle synthesis and analytical sample preparation [27,28]. In this study, gold nanoparticles (Au NPs) were produced using a femtosecond (fs) laser system operating at 800 nm. A high-purity gold target (99.99%) was immersed in a 10 mL glass vessel containing glacial acetic acid (ISOLABS).

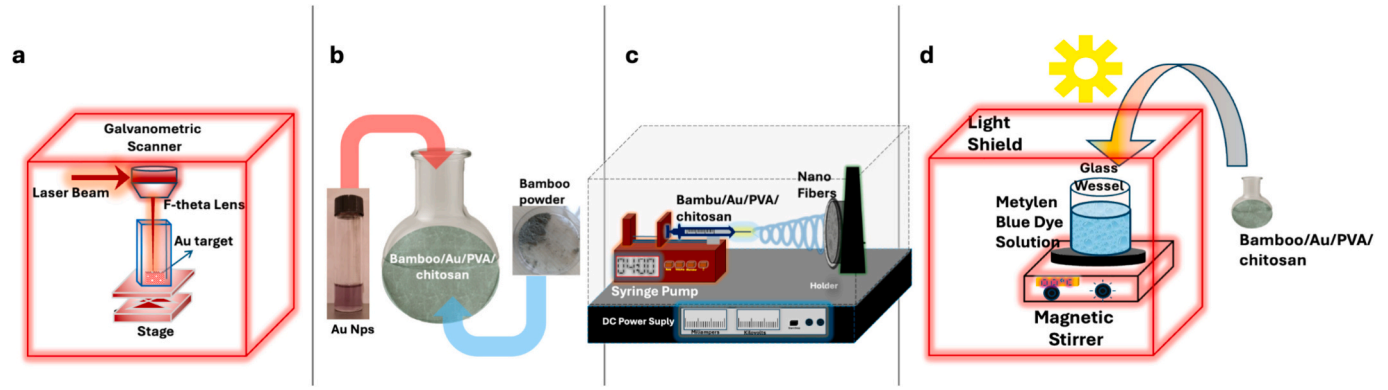

Fig. 1. Schematic illustration of the experimental workflow: (a) Au nanoparticles produced by laser ablation; (b) mixing of bamboo powder and Au NPs with poly (vinyl alcohol)/chitosan (PVA/CS) polymers; (c) nanofiber fabrication by electrospinning; (d) evaluation of the photocatalytic degradation of methylene blue using the obtained nanofibers. (For interpretation of the references to colour in this figure legend, the reader is referred to the web version of this article.)

The laser beam was focused onto the gold target for 15 min to initiate ablation, followed by an additional 30 min of irradiation under the same experimental conditions. This process yielded approximately 0.2 μg and 0.4 μg of Au NPs, which were used to prepare nanofiber composites with two different gold loadings. The corresponding samples were labeled Bamboo/Au/PVA/CS-1 and Bamboo/Au/PVA/CS-2, respectively. The detailed fs laser parameters employed in this work have been comprehensively reported in our previous publication [29].

2.3. Nanofiber production by electrospinning

Nanofibers were fabricated by incorporating bamboo powder and Au

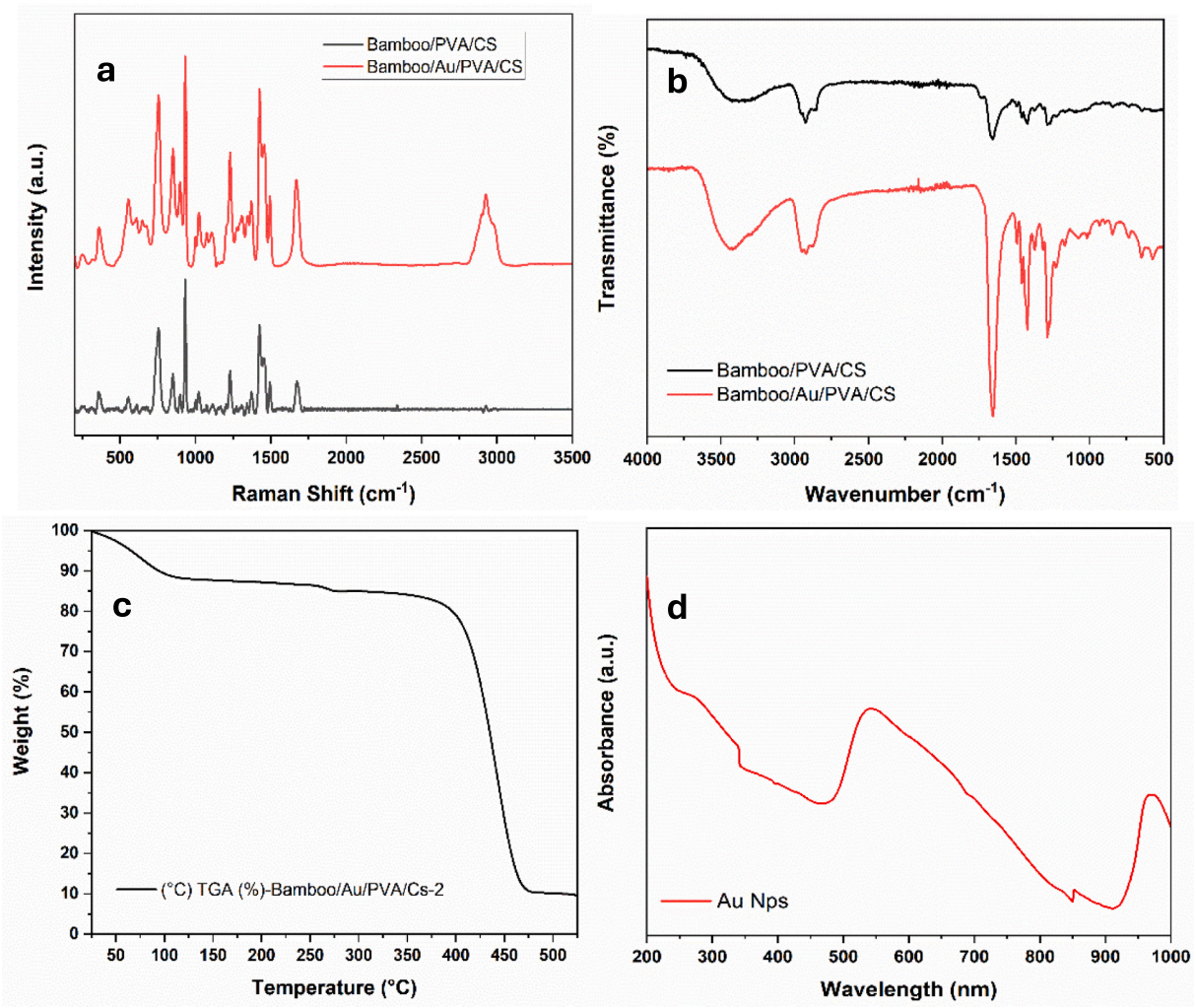

Fig. 2. (a) Raman spectra of Bamboo/PVA/CS and Bamboo/Au/PVA/CS-2 nanofibers. (b) FT-IR spectra of Bamboo/PVA/CS and Bamboo/Au/PVA/CS-2 nanofibers. (c) Thermogravimetric analysis (TGA) curve of Bamboo/Au/PVA/CS-2 nanofibers. (d) UV–Vis absorption spectrum of Au nanoparticles (Au NPs) produced by fs laser ablation.

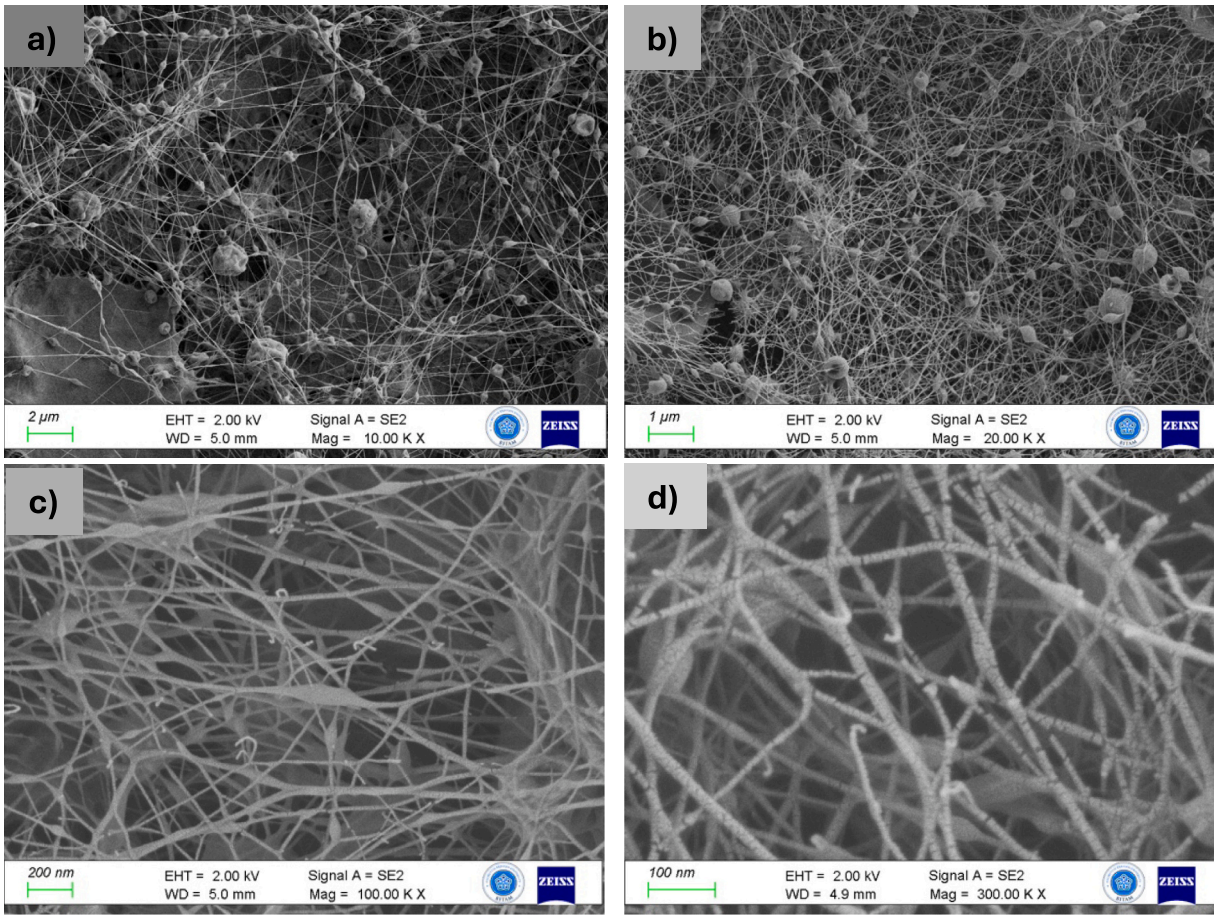

Fig. 3. FE-SEM images of electrospun nanofibers: (a) Bamboo/Au/PVA/CS-1 (10,000×), (b) Bamboo/Au/PVA/CS-2 (20,000×), (c) Bamboo/PVA/CS (100,000×), and (d) PVA/CS (300,000×). Scale bars: (a) 2 µm, (b) 1 µm, (c) 200 nm, (d) 100 nm.

nanoparticles into a poly(vinyl alcohol) (PVA)/chitosan (CS) polymer blend, using the electrospinning setup illustrated in Fig. 1c. In each experiment, 2 mL of the polymer solution was loaded into a 20 mL syringe mounted on a syringe pump, and the solution was fed through a stainless-steel needle (length, 15 mm; inner radius, 0.8 mm) at a constant flow rate of 0.1 mL/h. Electrospinning was carried out onto an aluminum foil collector positioned 15 cm from the needle tip. A high-voltage power supply (up to 50 kV) was used to apply an approximately 25 kV potential between the needle and the collector. All experiments were performed at room temperature. Two different Au loading levels were used in the bamboo/PVA/CS solutions to obtain the Bamboo/Au/PVA/CS-1 and Bamboo/Au/PVA/CS-2 nanofiber samples.

2.4. Photocatalytic evaluation of the produced nanofibers

The photocatalytic activity of the nanofibers produced in this study was investigated using methylene blue (MB) as a model pollutant. A 250 W metal-halide-halogen lamp (GE ARC250) was employed to simulate sunlight irradiation. For each test, 100 mL of MB solution in deionized water was prepared, and 0.05 g of the nanofiber photocatalyst was added (Fig. 1d). Prior to irradiation, the suspension was magnetically stirred in the dark for 20 min to establish adsorption–desorption equilibrium. During irradiation, 5 mL aliquots of the solution were collected every 20 min, and the relative MB concentration (C/C_0) was determined using a UV–Vis spectrophotometer. In this study, the photocatalytic performance of electrospun Bamboo/Au/PVA/CS-1, Bamboo/Au/PVA/CS-2, Bamboo/PVA/CS, and PVA/CS nanofibers toward MB degradation at pH 10 was systematically investigated.

2.5. Characterizations

In this study, the structural, chemical, thermal, and optical properties of the obtained samples were thoroughly examined. The absorption spectrum of Au nanoparticles (Au NPs) produced by fs laser ablation was recorded in the range of 200–1000 nm using a UV–Vis spectrophotometer (Shimadzu, Tokyo, Japan). Raman spectra (Renishaw, Hong Kong, China) and FT-IR spectra (Thermo Scientific, Nicolet iS20, USA) were obtained for the Bamboo/Au/PVA/CS-2 and Bamboo/PVA/CS nanofiber samples to analyze their vibrational and chemical characteristics. Thermogravimetric analysis (TGA) of Bamboo/Au/PVA/CS-2 nanofibers was performed between 25 °C and 525 °C (Setaram Labsys) to assess their thermal stability. Additionally, the surface morphology and fiber diameter distribution were investigated using FE-SEM (Zeiss, Gemini, Germany) to reveal the structural details of the fabricated nanofibers.

3. Results and discussion

3.1. Raman, FT-IR, TGA, and absorption spectra

Raman spectra of Bamboo/Au/PVA/CS-2 and Bamboo/PVA/CS nanofibers were recorded in the range of 200–3500 cm^{-1} to illustrate the vibrational characteristics of the samples. For both spectra, the most intense peak was observed at 924 cm^{-1}. The presence of Au NPs was found to significantly enhance peak intensities in the Raman spectrum. In addition, bamboo fibers contributed vibrational modes in the range of 1300–1600 cm^{-1} [30]. In the presence of the PVA/CS polymer mixture, Raman peaks were observed at 1233 cm^{-1} and 1431 cm^{-1}, which are

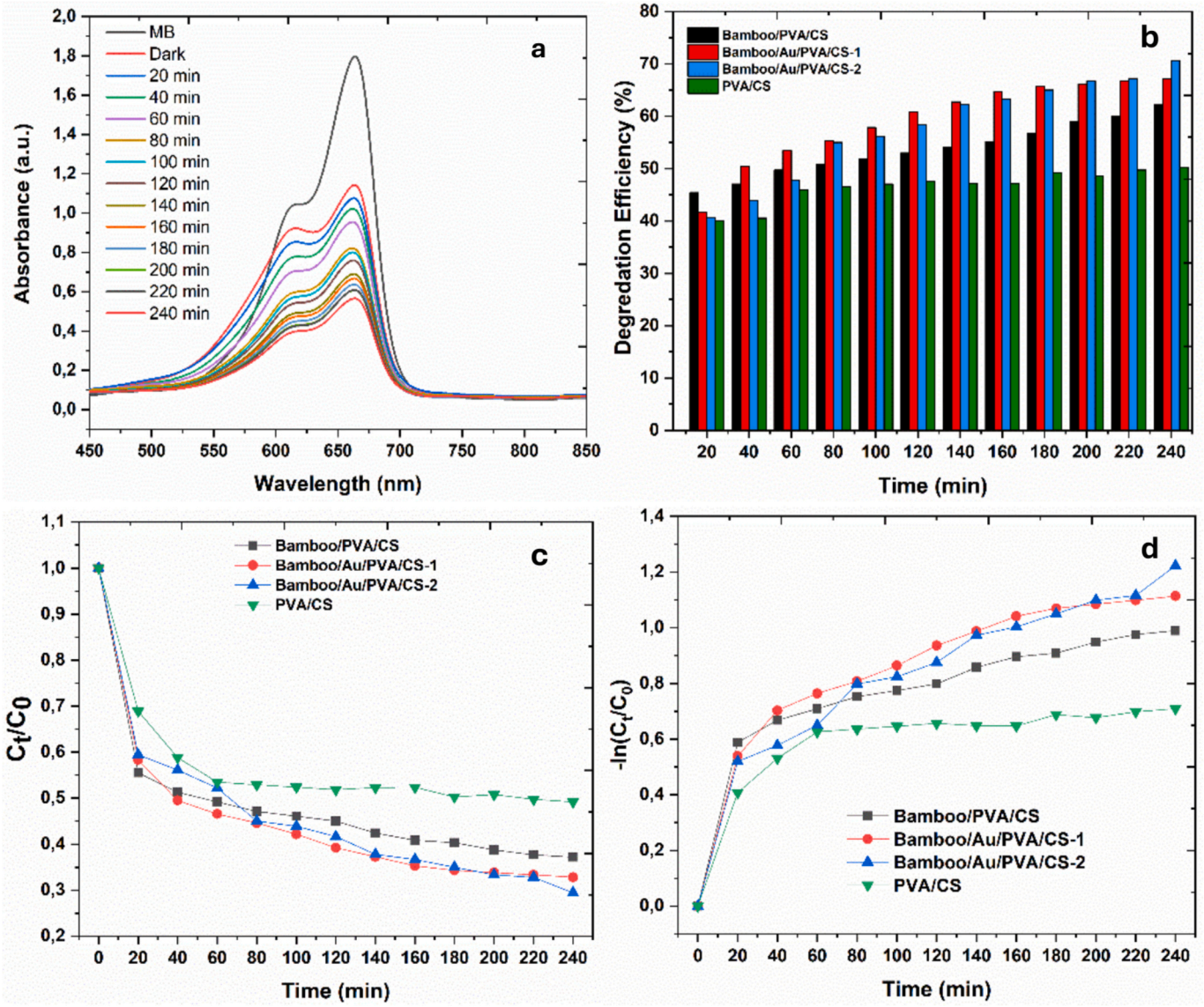

Fig. 4. Photocatalytic degradation of methylene blue (MB) under visible-light irradiation using PVA/CS-based nanofiber photocatalysts. (a) UV–Vis spectra of MB solution at different irradiation times in the presence of Bamboo/Au/PVA/CS-2 nanofibers. (b) Time-dependent photocatalytic degradation efficiency for Bamboo/Au/PVA/CS-1, Bamboo/Au/PVA/CS-2, Bamboo/PVA/CS, and PVA/CS nanofibers. (c) Plots of C_t/C_0 versus irradiation time. (d) Pseudo-first-order kinetic plots, $-\ln(C_t/C_0)$ versus time, were used to determine the apparent rate constants. (For interpretation of the references to colour in this figure legend, the reader is referred to the web version of this article.)

attributed to the bending vibrations of C—H and O—H groups [31]. For the Au-containing sample, an enhanced peak at 2922 cm^{-1} was observed, which has been reported in the literature as related to the dipole moment derivative associated with Au nanoparticles [32].

FT-IR spectra were recorded in the range of 500–4000 cm^{-1} to characterize the chemical features of the Bamboo/Au/PVA/CS-2 and Bamboo/PVA/CS nanofibers. The broad band in the 3600–3000 cm^{-1} region is assigned to N—H and O—H stretching vibrations. The bands at 3423 cm^{-1} and 2919 cm^{-1} are due to aliphatic C—H stretching vibrations arising from the CS and PVA polymers [33]. The peaks in the 1800–400 cm^{-1} region correspond to vibrations associated with the bamboo fibers [34]. The vibrational contribution of Au NPs was identified by the presence of bands in the 827–570 cm^{-1} range.

Thermogravimetric analysis (TGA) of Bamboo/Au/PVA/CS-2 nanofibers (Fig. 2c) revealed three main weight-loss stages. In the first stage, approximately 13% weight loss occurred between 25 °C and 100 °C. In the second stage, a further 4% weight loss was observed from 100 °C to 275 °C, which is attributed mainly to the removal of adsorbed and bound water. In the final stage, from 275 °C to 475 °C, a weight loss of about 73% was recorded due to the decomposition of the polymer components. The total weight loss was approximately 90%, indicating the organic nature of the nanofiber matrix.

The optical absorption of the Au NPs was evaluated by UV–Vis spectroscopy. As shown in Fig. 2d, the absorption spectrum exhibits a pronounced band in the visible region, confirming the presence of a localized surface plasmon resonance (LSPR) effect, in agreement with previous reports. The maximum absorption peak was observed at approximately 540 nm, a characteristic wavelength of colloidal gold nanoparticles (Au NPs), indicating their effective formation via femtosecond (fs) laser ablation.

3.2. FE-SEM morphology of nanofibers

The morphological features of the electrospun nanofibers were examined by field-emission scanning electron microscopy (FE-SEM). Bamboo powder and Au nanoparticles were successfully incorporated

Table 1
Kinetic constants and photocatalytic degradation efficiencies of PVA/CS-based nanofiber photocatalysts at pH 10.

Photocatalyst	Kinetic constants, k (min^{-1})	Photocatalytic degradation efficiency (% in 240 min)
PVA/CS	0.0021	50.27
Bamboo/PVA/CS	0.0024	62.16
Bamboo/Au/PVA/CS-1	0.0034	67.15
Bamboo/Au/PVA/CS-2	0.0038	70.55

into the PVA/CS polymer matrix, as evidenced by the surface texture and contrast variations observed in the FE-SEM images. The nanofibers in the Bamboo/Au/PVA/CS samples (Fig. 3a, b) exhibited relatively uniform diameters, with most fibers falling in the range of approximately 500–750 nm. At higher magnification (Fig. 3a–c), nanoscale features attributed to the embedded Au nanoparticles were observed, with estimated sizes on the order of 10–16 nm.

The nanofiber mats exhibited a randomly oriented, nonwoven morphology, characteristic of electrospun structures. The coexistence of PVA and chitosan, a biocompatible polymer blend, enabled the formation of continuous, bead-free fibers under an applied electric field of 25 kV. For the PVA/CS-based nanofibers without Au loading (Fig. 3d), the fiber diameters were slightly different, typically in the range of about 15–25 nm, reflecting the influence of the polymer composition and electrospinning conditions on fiber formation.

The plasmonic activity of the Bamboo/Au/PVA/CS nanofibers strongly depends on the accessibility of Au nanoparticles at the nanofiber–water interface. FE-SEM observations indicate that Au nanoparticles are not fully encapsulated within the polymer matrix but are predominantly distributed at or near the nanofiber surface, as evidenced by surface contrast variations and nanoscale protrusions. This surface-exposed configuration is further supported by the pronounced LSPR absorption in the UV–Vis spectra and the marked enhancement in photocatalytic degradation kinetics. Such near-surface localization facilitates efficient light–matter interaction and interfacial charge transfer, enabling LSPR-assisted generation of reactive species under visible-light irradiation [35].

3.3. Photocatalysis results

The photocatalytic activity of the nanofiber samples was evaluated through the degradation of methylene blue (MB) under visible-light irradiation. The 240-min photocatalytic experiments confirmed that the Bamboo/Au/PVA/CS-2 nanofibers exhibited the highest MB degradation efficiency among all samples (Fig. 4a). The degradation efficiencies (%) and apparent kinetic rate constants (k) for Bamboo/Au/PVA/CS-1, Bamboo/Au/PVA/CS-2, Bamboo/PVA/CS, and PVA/CS nanofibers were calculated from the temporal concentration profiles and are summarized in Fig. 4b and Table 1.

The degradation kinetics of MB were analyzed using a pseudo-first-order model according to:

$$\ln (C_t/C_0) = -kt \quad (1)$$

where time (t), the initial equilibrium concentration of methylene blue (C_o), the concentration at a given time (C_t), and the apparent rate constant (k). The parameter t represents the reaction time in minutes, corresponding to the methylene blue concentration measured at each interval. The logs of Bamboo/Au/PVA/CS-1, Bamboo/Au/PVA/CS-2, Bamboo/PVA/CS, and PVA/CS with time have been plotted in Fig. 4d.

As summarized in Table 1, both the degradation efficiencies and the apparent rate constants (k) increased with the incorporation of bamboo powder and Au nanoparticles into the PVA/CS matrix. The k value increased from 0.0021 min^{-1} for PVA/CS to 0.0024 min^{-1} for Bamboo/PVA/CS, indicating a beneficial contribution of bamboo-derived carbon to the photocatalytic activity. Further enhancement was achieved by Au loading, with k values of 0.0034 min^{-1} and 0.0038 min^{-1} for Bamboo/Au/PVA/CS-1 and Bamboo/Au/PVA/CS-2, respectively. Overall, the Bamboo/Au/PVA/CS-2 sample exhibited the highest performance, with a rate constant approximately 1.8 times higher than that of PVA/CS and a degradation efficiency of 70.55% after 240 min.

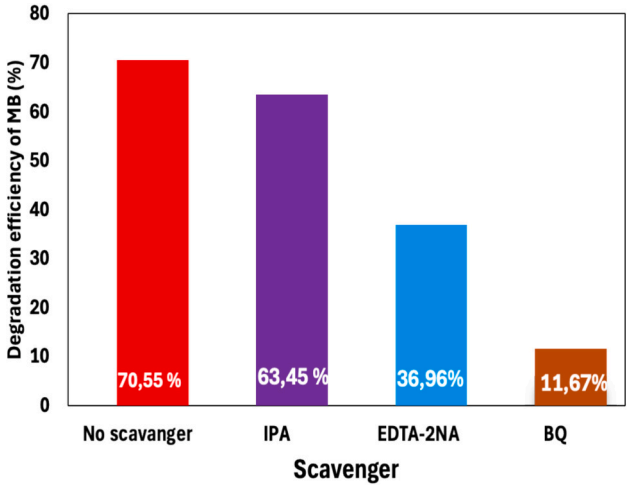

Fig. 5. Effect of different radical scavengers on the photocatalytic degradation of methylene blue (MB) over Bamboo/Au/PVA/CS-2 nanofiber photocatalyst after 240 min of visible-light irradiation: no scavenger, isopropyl alcohol (IPA, •OH scavenger), ethylenediaminetetraacetic acid disodium salt (EDTA-2Na, h^+ scavenger), and p-benzoquinone (BQ, O_2^- scavenger). (For interpretation of the references to colour in this figure legend, the reader is referred to the web version of this article.)

Under visible-light irradiation, recent studies on plasmonic nanofibers and related metal-nanoparticle-decorated photocatalytic systems report a range of apparent first-order rate constants (k) for organic dye degradation, providing useful benchmarks for evaluating performance. For example, electrospun Ag–TiO_2 nanofibers have shown enhanced photocatalytic activity with k values on the order of 4.2×10^{-3} min^{-1} under visible-light conditions [36], situating them in a similar range to the Bamboo/Au/PVA/CS-2 system presented here. Additional works on plasmonic Ag–TiO_2 nanofibers report rate constants up to ~1.3×10^{-2} min^{-1} for methylene blue degradation under broad visible illumination, reflecting the influence of nanoparticle loading and support architecture on photocatalytic kinetics [37]. Compared with these systems, the Bamboo/Au/PVA/CS-2 nanofibers exhibit a rate constant of 0.0038 min^{-1} under visible light, which is at the lower end or comparable with reported values while employing a fully biodegradable, surfactant-free nanofiber matrix.

Scavenger tests were performed to identify the main reactive species involved in MB degradation over Bamboo/Au/PVA/CS-2 nanofiber photocatalysts. As shown in Fig. 5, different scavenging agents were added to the MB solution: isopropyl alcohol (IPA, 5 mmol L^{-1}) as a hydroxyl radical (•OH) scavenger, ethylenediaminetetraacetic acid disodium salt (EDTA-2Na, 5 mmol L^{-1}) as a hole (h^+) scavenger, and p-benzoquinone (BQ, 1 mmol L^{-1}) as a superoxide radical ($•O_2^-$) scavenger. The degradation of MB was monitored for 240 min in the presence and absence of these scavengers.

In the absence of scavengers, the maximum degradation efficiency reached 70.55%. Upon the addition of IPA, the degradation efficiency slightly decreased to 63.45%, indicating that •OH radicals contribute to the photocatalytic process but are not the dominant reactive species. In contrast, the presence of EDTA-2Na reduced the degradation efficiency to 36.96%, showing that photogenerated holes (h^+) play a significant role in the MB degradation mechanism. The most pronounced inhibition was observed upon addition of BQ, with the degradation efficiency

Table 2
Bamboo Nanofiber Photocatalysis Papers.

No	Paper / Year	Material System	Key Method	Application	Main Findings
1	Zhang et al., 2021 [38]	Bamboo-derived carbon aerogel + TiO_2	Carbonization + TiO_2 coating	Dye degradation (MB)	High degradation efficiency combined with strong adsorption and UV photocatalysis
2	Guan et al., 2024 [39]	TiO_2/TiC on bamboo chopsticks	Coating/calcination	Floatable photocatalyst, dye removal	Easy recovery; powerful solar-driven photocatalysis
3	Chabalala et al., 2021 [40]	Photocatalytic nanofiber membranes	Electrospinning + nanoparticle loading	Water treatment	Comprehensive analysis of membrane fabrication and performance
4	Zhang et al., 2020 [41]	Nanobamboo TiO_2 arrays	Hydrothermal growth, defect engineering	Visible-light photocatalysis	Increased charge separation and apparent absorption as a result of flaw structures
5	Sun et al., 2022 [42]	Nanotechnology on bamboo materials (review)	Nanocellulose isolation, nanoparticles	Environmental applications	Overview of nanotech strategies applied to bamboo
6	Kwon et al., 2021 [43]	TiO_2-grafted bamboo cellulose acetate fibers	Grafting + fiber fabrication	Phenol degradation + filtration	High stability and dual photocatalytic/filtration ability
7	Yan et al., 2024 [44]	Bamboo-based ZnO/WO_3 heterojunction	In-situ growth on bamboo	Dye & formaldehyde degradation	Strong visible-light activity; effective heterojunction formation
8	Hassaan et al., 2023 [45]	General photocatalyst review	Mechanism analysis	Environmental remediation	Clear explanation of ROS mechanisms & catalyst design principles

dropping to 11.67%. This strong suppression demonstrates that superoxide radicals ($\bullet O_2^-$) are the primary reactive species responsible for MB degradation over the Bamboo/Au/PVA/CS-2 photocatalyst.

In Table 2, the existing studies in the literature presented [38–47]. In this study, laser ablation-based nanoparticle manufacturing, a green synthesis method, was employed and introduced into the PVA/Cs polymer matrix. A clean, surfactant-free, and highly controlled method for producing stable colloidal Au nanostructures with precise size distribution and high purity is laser ablation-based gold nanoparticle manufacturing. Unlike chemical production, laser ablation avoids hazardous reducing agents and residual pollutants, making the resultant nanoparticles especially suited for biological, environmental, and optical applications. By combining the mechanical strength, biocompatibility, and film-forming capacity of PVA/CS with the plasmonic, catalytic, and antimicrobial properties of gold, the incorporation of these laser-generated Au nanoparticles into a PVA/CS polymer matrix greatly improves the functional properties of the composite. Such nanocomposites offer potential for advanced applications, including photocatalysis, antimicrobial surfaces, sensing, drug delivery, and optoelectronics [39,40,42]. As a whole, this technique provides a sustainable pathway for creating high-performance hybrid materials.

4. Conclusion

In this study, composite nanofibers based on PVA/CS, Bamboo/PVA/CS, Bamboo/Au/PVA/CS-1, and Bamboo/Au/PVA/CS-2 were successfully fabricated by electrospinning. Gold nanoparticles (Au NPs) synthesized by laser ablation in liquid were incorporated into the polymer matrix to enhance photocatalytic performance. The nanofibers were designed to degrade methylene blue (MB), a toxic dye frequently discharged into the environment by the textile and dyeing industries. Comprehensive characterization by FE-SEM, FT-IR, Raman spectroscopy, TGA, and UV–Vis spectroscopy confirmed the formation of the nanocomposite structures and the effective dispersion of bamboo-derived components and Au NPs within the PVA/CS polymer matrix.

Photocatalytic tests showed that the biodegradable nanofibers exhibit significant MB degradation, with the Bamboo/Au/PVA/CS-2 sample displaying the highest activity, achieving a degradation efficiency of 70.55% and an apparent pseudo-first-order rate constant of 0.0038 min^{-1} at pH:10. These results indicate strong potential for the use of bamboo-based, Au NP-modified nanofibers in wastewater treatment and environmental remediation. Overall, the integration of bamboo-derived components with surfactant-free Au NPs in a PVA/CS matrix offers a promising, eco-friendly route to efficient, visible-light-driven photocatalytic materials. The findings contribute to the development of sustainable, nano-enabled water purification technologies and highlight composite nanofibers as multifunctional candidates for future environmental applications.

CRediT authorship contribution statement

Yasemin Gündoğdu Kabakci: Visualization, Software, Methodology, Investigation. **Nezihe Mehtap:** Validation, Software, Methodology, Investigation. **M.A.Basyooni-M. Kabatas:** Writing – review & editing, Writing – original draft, Visualization, Methodology, Investigation. **Hamdi Şükür Kiliç:** Validation, Supervision, Software, Resources, Project administration.

Funding

Selcuk University Scientific Research Project (BAP) Coordination under project no. 22401093.

Declaration of competing interest

The authors declare that they have no known competing financial interests or personal relationships that could have influenced the work reported in this paper.

Data availability

Data will be made available on request.

References

[1] F. Karimi, et al., Removal of metal ions using a new magnetic chitosan nano-bio-adsorbent; a powerful approach in water treatment, Environ. Res. 203 (2022) 111753.
[2] Y. Orooji, et al., Heterogeneous UV-switchable Au nanoparticles decorated tungstophosphoric acid/TiO2 for efficient photocatalytic degradation process, Chemosphere 281 (2021) 130795.
[3] K.-t. Lau, et al., Properties of natural fibre composites for structural engineering applications, Compos. Part B 136 (2018) 222–233.
[4] V.K. Thakur, M.K. Thakur, R.K. Gupta, Raw natural fiber–based polymer composites, Int. J. Polym. Anal. Charact. 19 (3) (2014) 256–271.
[5] A. Varghese, V. Mittal, Polymer Composites with Functionalized Natural Fibers, Woodhead Publishing, Cambridge, United Kingdom, 2018, pp. 157–186.
[6] H. Ran, et al., Preparation of iron oxide-loaded bamboo charcoals and their trinitrotoluene red water treatment, Desalin. Water Treat. 57 (19) (2016) 8739–8747.
[7] B. Wang, et al., Synthesis, characterization, and photocatalytic properties of bamboo charcoal/TiO2 composites using four sizes powder, Materials 11 (5) (2018) 670.
[8] C.-S. Chou, et al., Design and fabrication of multi-functional working electrodes with TiO2/CZTSe/bamboo-charcoal-powder composite particles for use in dye-sensitized solar cells, Sol. Energy 126 (2016) 231–242.
[9] A. Muxika, et al., Chitosan as a bioactive polymer: processing, properties and applications, Int. J. Biol. Macromol. 105 (2017) 1358–1368.
[10] M. Dash, et al., Chitosan—a versatile semi-synthetic polymer in biomedical applications, Prog. Polym. Sci. 36 (8) (2011) 981–1014.

[11] N.K. Abdulla, et al., Silver based hybrid nanocomposite: a novel antibacterial material for water cleansing, J. Clean. Prod. 284 (2021) 124746.
[12] M. Majeed, K.R. Hakeem, R.U. Rehman, Synergistic effect of plant extract coupled silver nanoparticles in various therapeutic applications-present insights and bottlenecks, Chemosphere 288 (2022) 132527.
[13] Y. Gao, et al., The polarization effect in surface-plasmon-induced photocatalysis on Au/TiO2 nanoparticles, Angew. Chem. 132 (41) (2020) 18375–18380.
[14] K. Kalantari, et al., Evaluation of heavy metals removal by cross-linked (polyvinyl alcohol/chitosan/magnetic) nano fibrous membrane prepared by electro spinning technique, Desalin. Water Treat. 98 (2017) 266–275.
[15] E. Sapountzi, et al., Gold nanoparticles assembly on electrospun poly (vinyl alcohol)/poly (ethyleneimine)/glucose oxidase nanofibers for ultrasensitive electrochemical glucose biosensing, Sens. Actuators B 238 (2017) 392–401.
[16] X. Zhang, et al., Plasmonic photocatalysis, Rep. Prog. Phys. 76 (4) (2013) 046401.
[17] Y. Tian, T. Tatsuma, Mechanisms and applications of plasmon-induced charge separation at TiO2 films loaded with gold nanoparticles, J. Am. Chem. Soc. 127 (20) (2005) 7632–7637.
[18] K. Awazu, et al., A plasmonic photocatalyst consisting of silver nanoparticles embedded in titanium dioxide, J. Am. Chem. Soc. 130 (5) (2008) 1676–1680.
[19] M.L. Brongersma, N.J. Halas, P. Nordlander, Plasmon-induced hot carrier science and technology, Nat. Nanotechnol. 10 (1) (2015) 25–34.
[20] K. Qian, et al., Surface plasmon-driven water reduction: gold nanoparticle size matters, J. Am. Chem. Soc. 136 (28) (2014) 9842–9845.
[21] C. Boerigter, et al., Evidence and implications of direct charge excitation as the dominant mechanism in plasmon-mediated photocatalysis, Nat. Commun. 7 (1) (2016) 1–9.
[22] D. Saha, et al., Fabrication of electrospun nanofiber composite of g-C3N4 and au nanoparticles as plasmonic photocatalyst, Surf. Interfaces 26 (2021) 101367.
[23] Y. Zhang, et al., Surface-plasmon-driven hot electron photochemistry, Chem. Rev. 118 (6) (2017) 2927–2954.
[24] P.S. Delgado, et al., The potential of bamboo in the design of polymer composites, Mater. Res. 15 (4) (2012) 639–644.
[25] M. Adamu, M.R. Rahman, S. Hamdan, Formulation optimization and characterization of bamboo/polyvinyl alcohol/clay nanocomposite by response surface methodology, Compos. Part B Eng. 176 (2019) 107297.
[26] M. Adamu, et al., Impact of polyvinyl alcohol/acrylonitrile on bamboo nanocomposite and optimization of mechanical performance by response surface methodology, Constr. Build. Mater. 258 (2020) 119693.
[27] A. Menazea, Femtosecond laser ablation-assisted synthesis of silver nanoparticles in organic and inorganic liquids medium and their antibacterial efficiency, Radiat. Phys. Chem. 168 (2020) 108616.
[28] P.M. Khaniabadi, et al., Structure, morphology and absorption characteristics of gold nanoparticles produced via PLAL method: role of low energy X-ray dosage, Surf. Interfaces 24 (2021) 101139.
[29] Y. Gündoğdu, et al., Femtosecond laser-induced production of ZnO@ Ag nanocomposites for an improvement in photocatalytic efficiency in the degradation of organic pollutants, Opt. Laser Technol. 170 (2024) 110291.
[30] R. Ramful, et al., Investigating the effect of smoke treatment on hygroscopic characteristics of bamboo by FTIR and raman spectroscopy, Materials 15 (4) (2022) 1544.
[31] D.F. Katowah, et al., Ultrasensitive QCM sensor development for monitoring of methyl orange dye in aqueous phase based on novel cross-linked chitosan/PVA/GO/Ce-ZnO nanocomposite film, Mater. Sci. Eng. B 297 (2023) 116804.
[32] M. Baia, et al., Multilayer structures of self-assembled gold nanoparticles as a unique SERS and SEIRA substrate, ChemPhysChem 10 (7) (2009) 1106–1111.
[33] S.K. Mishra, J. Ferreira, S. Kannan, Mechanically stable antimicrobial chitosan–PVA–silver nanocomposite coatings deposited on titanium implants, Carbohydr. Polym. 121 (2015) 37–48.
[34] Z. Liu, et al., Preparation of bamboo-shaped BiVO4 nanofibers by electrospinning method and the enhanced visible-light photocatalytic activity, J. Alloys Compd. 651 (2015) 29–33.
[35] P. Shahini, A.A. Ashkarran, Immobilization of plasmonic Ag-Au NPs on the TiO2 nanofibers as an efficient visible-light photocatalyst, Colloids Surf. A Physicochem. Eng. Asp. 537 (2018) 155–162.
[36] E.W. Awin, et al., Plasmon enhanced visible light photocatalytic activity in polymer-derived TiN/Si-OCN nanocomposites, Mater. Des. 157 (2018) 87–96.
[37] P. Pascariu, et al., Innovative Ag–TiO2 nanofibers with excellent photocatalytic and antibacterial actions, Catalysts 11 (10) (2021) 1234.
[38] J. Zhang, et al., A TiO2 coated carbon aerogel derived from bamboo pulp fibers for enhanced visible light photo-catalytic degradation of methylene blue, Nanomaterials 11 (1) (2021) 239.
[39] S. Guan, et al., Achieving water-floatable photocatalyst on recycled bamboo chopsticks, Sci. Rep. 14 (1) (2024) 9496.
[40] M.B. Chabalala, et al., Photocatalytic nanofiber membranes for the degradation of micropollutants and their antimicrobial activity: recent advances and future prospects, Membranes 11 (9) (2021) 678.
[41] Y. Zhang, et al., Defective titanium dioxide nanobamboo arrays architecture for photocatalytic nitrogen fixation up to 780 nm, Chem. Eng. J. 401 (2020) 126033.
[42] H. Sun, et al., Nanotechnology application on bamboo materials: a review, Nanotechnol. Rev. 11 (1) (2022) 1670–1695.
[43] M. Kwon, J. Kim, J. Kim, Photocatalytic activity and filtration performance of hybrid tio2-cellulose acetate nanofibers for air filter applications, Polymers 13 (8) (2021) 1331.
[44] X. Yan, et al., Nanoarchitectonics of bamboo-based heterojunction photocatalyst for effective removal of organic pollutants, Chem. Eng. J. 495 (2024) 153431.
[45] M.A. Hassaan, et al., Principles of photocatalysts and their different applications: a review, Top. Curr. Chem. 381 (6) (2023) 31.
[46] Z.F. Yin, et al., Recent progress in biomedical applications of titanium dioxide, Phys. Chem. Chem. Phys. 15 (14) (2013) 4844–4858.
[47] X. Zhang, et al., In situ hydrothermal growth and in vitro biocompatibility of TiO2 nanowires grown on TiO2 nanoparticle compacts as novel supportive substrates, Mater. Technol. 37 (13) (2022) 2758–2765.